Design of an Active Magnetic Bearing for the Identification of Static and Dynamic Performances of a self-Aligning Hydrodynamic Journal Bearing

Jean-Yves Roger[(a)], Mohamed-Amine Hassini[(a)], Lucien Desprez[(a)], Jarir Mahfoud[(b)]

[(a)]EDF R&D, 7 Gaspard Monge, Palaiseau, France

[(b)] University of Lyon, INSA-Lyon, CNRS UMR5259, LaMCoS, F-69621 Villeurbanne Cedex, France

1 Abstract

Large Self-Aligning Hydrodynamic Journal Bearings (SAHJB) are used in many heavy-duty rotating machines such as steam turbines. In an EPR2 nuclear power plant, their diameter can reach up to 800mm. To test a representative small scale of such bearings (100mm diameter), a test rig is being designed where the SAHJB is mounted in the middle of a shaft supported by two active magnetic bearings (AMB) at its ends and operated up to 5000 rpm. The role of the AMBs is to apply enough static load to the SAHJB to obtain a Sommerfeld number on the tested SAHJB equivalent to the one used on the real turbine. The AMBs will also be used to impart small perturbations to the rotor movement in order to identify the stiffness and damping coefficient of the SAHJB for different bearing-rotor misalignment. To evaluate the forces in the magnetic bearing, a finite element FE approach was implemented using the inhouse software code_Carmel. Both a simplified structure of an electromagnet (a U shape core attracting and an I shape core) and a realistic magnetic bearing (8 magnetic poles) have been modelled. On the simplified structure, results of FE calculations with linear hypothesis on magnetic materials (7000 times vacuum permeability) are in very good agreement with the results of an equivalent analytical model. These theoretical results are also in good agreement with experimental data. The same FE model was utilized to evaluate the effect of the non-linearity of the magnetic core. When the saturation of the magnetic core occurs, the forces available within the airgap between the fix part and the mobile part of the electromagnet, decrease. For low saturation of the magnetic core, the obtained forces are in good agreement with the analytic model results. Considering the actual magnetic bearing, the same type of calculations was carried out, allowing evaluations of the effect of magnetic non-linearity and geometrical dimensions on bearing performances. These elements are used to evaluate both the actual forces available within the bearing and the optimal domain of use of the AMB in a pre-design stage.

Keywords: *AMB, design, Hydrodynamic bearing*

1. Introduction

The objective of the paper is to give details on the design of a magnetic bearing which will be used to analyze the static and dynamic behavior of Self-Aligning Hydrodynamic Journal Bearings. These bearings are heavily loaded to prevent any hydrodynamic instability (whirl instability). They are also capable to accommodate large amount of rotor to bearing misalignment. Such feature is important to ensure bearing reliability and reduce alignment requirements which in turn facilitate maintenance operations.

A Thermo-Elasto-Hydrodynamic numerical model implemented within LEGOS, a Python library developed by EDF R&D to predict the static and dynamic behavior of hydrodynamic and hydrostatic bearings. The pressure field within the oil film gap is predicted using a finite volumes model that solves the generalized Reynolds equation while considering film rupture and reformation. The Reynolds equation is coupled with a 3D Energy equation to predict the temperature field within the oil film. This hydrodynamic model (Reynolds and energy equation) is also coupled with a finite element thermo-mechanical model of the bearing solid parts using a Neumann-Dirichlet strategy to solve the conjugate heat transfer problem between the oil film and the bearing and predict its elastic deformation that impact the oil film gap. The details of the model can be found in .

Like any theoretical model, it requires experimental data are necessary to validate the developed model. The validation is performed with respect to static performances, i.e., pressure field, inlet and outlet temperature, oil flow rate, etc.., and dynamic behavior, i.e., the stiffness and damping coefficients. The latter are usually identified by imparting small perturbation to the bearing using a hydraulic or electrical shaker and measuring the generated force. It is also possible to impart the perturbation directly to the rotor usually through ball bearing [2] or using a highly stiff

hydrostatic bearing [3] or AMBs [4]. Because of the SAHJB unique feature to self-align, AMBs were selected to apply the necessary vertical load, generate a controlled misalignment while imparting small perturbation to the rotor. This will lead to geometrical variations of the airgap within the magnetic bearing and of the magnetic behavior of the actuator.

To achieve these goals, numerical studies were carried out to optimize the design of the AMBs and to evaluate the effect of misalignment on their performances. The design of the magnetic bearing followed two steps: a first step was to design a simple electromagnet actuator to evaluate the methods and tools that will be used. The second step was to design the full-scale magnetic bearing.

2. Test rig description

Figure 1 present the designed test rig that will be used to carry out the validation of the SAHJB theoretical model. A rotor operated up to 5000 rpm is supported by two AMBs at its ends. It is driven by an electric motor using a flexible coupling. Both the electric motor and the coupling are not represented. The SAHJB is a 100 mm diameter and is placed between the AMBs. The bearing is lubricated using an ISOVG 68 mineral oil. The active surface of the hydrodynamic bearing is coated using white metal. Small holes are machined within the lower lobe to measure the hydrodynamic pressure that build up with the thin film fluid. The bearing is also equipped with temperature probes that measure the temperature of the solid part just underneath the coating. The bearing has two pockets, one on the leading edge and one on the trailing edge of the lower lobe. The oil is supplied to the bearing through the leading-edge pocket. The lower lobe is supported using a lower plate that allow the bearing to tilt in the two directions perpendicular to the bearing axial axis. The other plates are not in contact with the bearing casing. The flexible couple will ensure the rotor axial constraint since the axial forces are negligible.

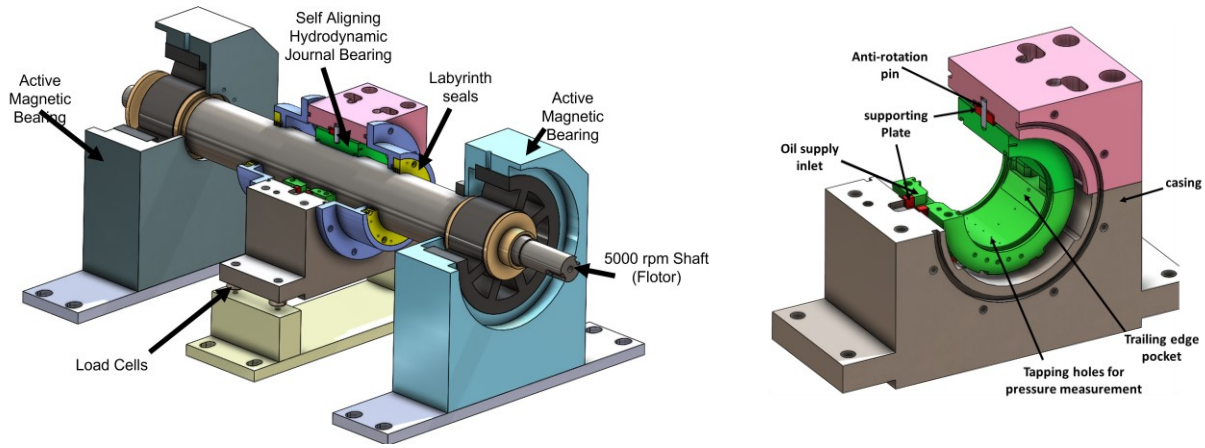

Figure 1 View of the test rig. On the left a rotor supported by two AMBs and a central SAHJB. On the right, view of the SAHJB

3. Test case

In order to evaluate the design process a first modelling has been carried out on a simple structure. Theorical and experimental approaches have been done.

3.1. Numerical approach

The electromagnet actuator design is depicted in Figure 2. The geometry and the mesh are generated using the Salome platform using the shaper and smesh modules (website Salome-platform [5]). The shaper module allows to draw a parametric model which will be used especially for optimizing the design. The generated meshes were both 2D and 3D models. The 2D modelling is sufficient to evaluate the forces but 3D modeling were also used to validate the computation in that case also. The method used to evaluate the forces is the well-known virtual work method.

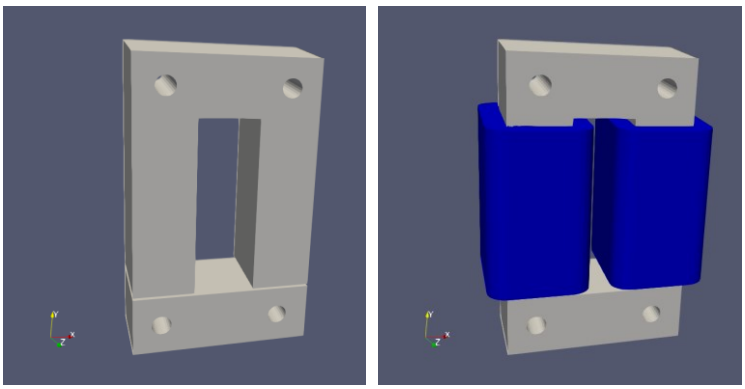

Figure 2 Design of the first electromagnet U-shape and I-shape magnetic core and winding

To compare the forces obtained using Finites Elements computation, we use the simplified analytical forces from [6]:

$$F = \mu_0 . A_0 . \left(\frac{N.I}{2.\delta_0}\right)^2 \quad (1)$$

Where, F is the total forces available in the airgap, μ_0 the vacuum permeability, A_0 the area of magnetic pole, N the number of turns of windings, I the applied current and δ_0 is the nominal radial clearance.

3D modeling has been made, one with linear magnetic properties and two with the non-linear properties of M270-35A electrical steel material, with and without the holes in the I and U shape. With linear properties values are very close to the theorical forces. With the non-linearity considered, we see a large reduction of the available forces for high current values due to saturation and small effects of holes in the magnetic circuit on the force value. As shown in Figure 3, the finite element model is in good agreement with the analytical solution in the simple case of a single electro-magnet. The effect of holes is also negligeable.

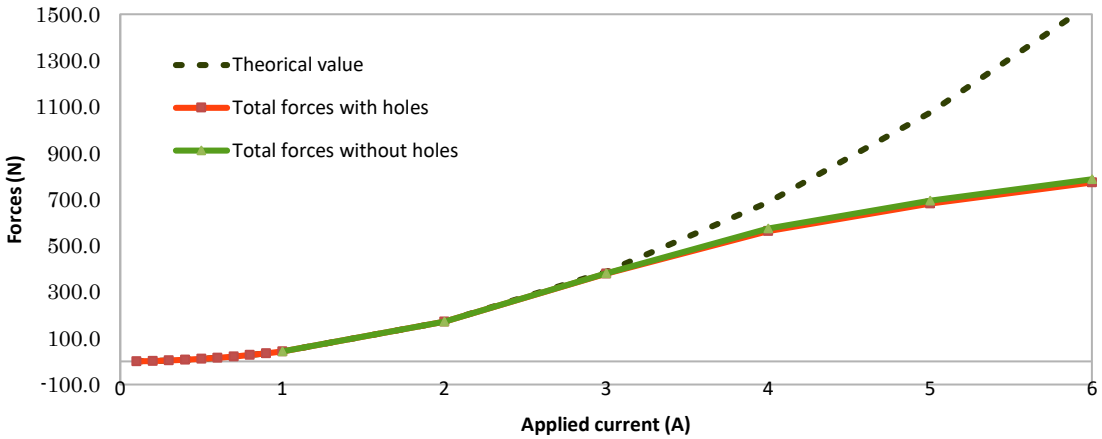

Figure 3 Forces values with theoretical approach and EF approach with and without holes in the magnetic circuit

4. Magnetic bearing

For this study, we choose to use a heteropolar-type radial AMB with an 8 poles structure (Figure 4). The aim of the study is to design the magnetic bearing according to the required performances. As a base design, we used some fixed dimensions as: an airgap of 0.5 mm and an outer diameter of the rotor shaft of 55mm. In addition, an analytical approach set the number of turns of each winding to 191 turns of a 1.1mm² wire. Thus, the minimum size of the winding can be estimated. Other dimensions, as the inner and outer diameter of the stator, the outer diameter of the rotor and the height of the teeth, are parameters of the study. The size of the slot has also been considered a possible parameter of design.

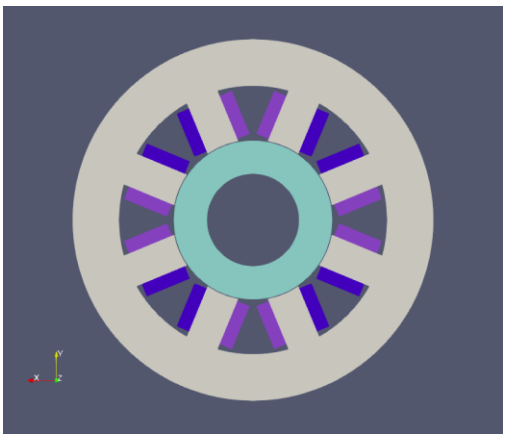

Figure 4 Base design of the first magnetic bearing

4.1 Effect of teeth spanning on available forces

A study of the effects of the teeth form have been done, considering all other dimensions fixed, and especially the surface used to compute the forces in each case. We have modeled: case (a): teeth are rectangular (0.0° between radial direction and the border of tooth, case (c): slots are rectangular (22.5° between radial direction and the border of tooth) and a case (c) which is in between (11.25°). The computed forces are presented on Figure 6.

The opening of each tooth increases the value of the available forces. The larger is the teeth at his root, the higher is the force. This can be explained both by the reduction of the saturation in the teeth and also by the reduction of the reluctance value due to the length reduction of the magnetic iso-value lines.

For the next optimization, the larger opening will be used, corresponding to a rectangular slot, case (c).

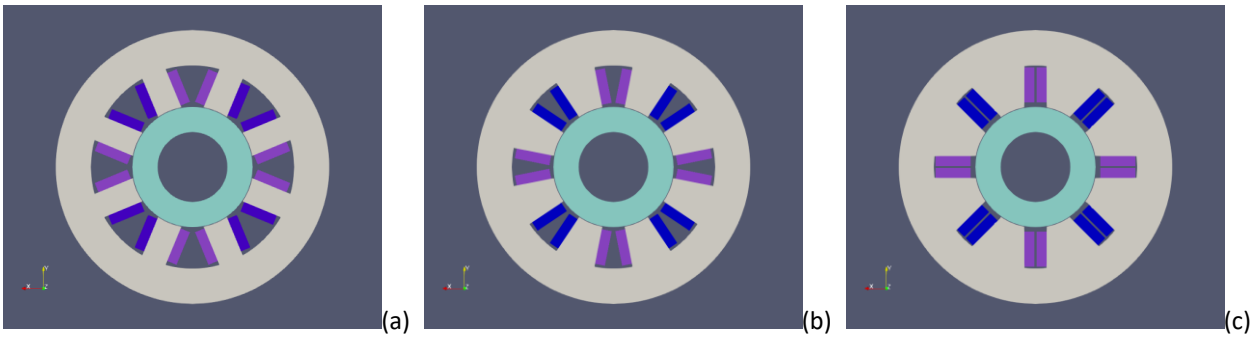

Figure 5 Study of the teeth spanning for three dimensions (a): 0.0° (b): 11.25° - (c): 22.5°

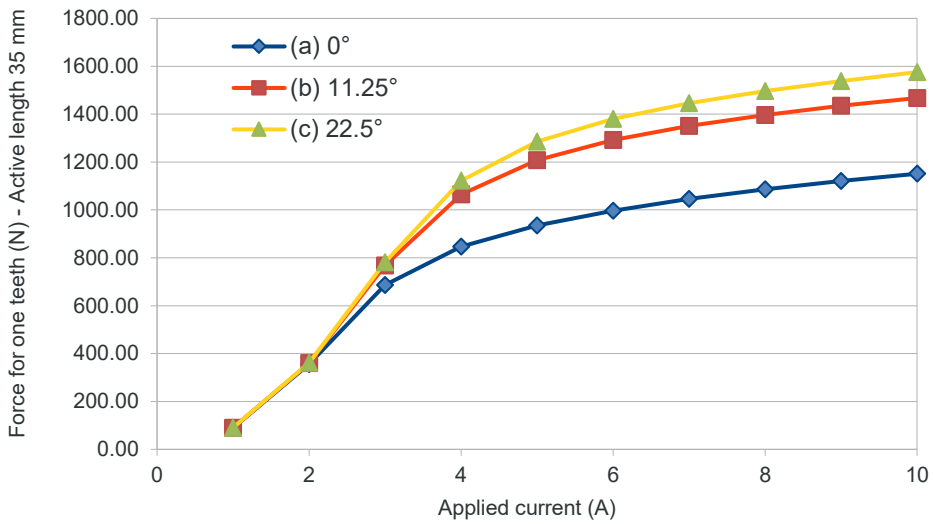

Figure 6 Forces obtained with three teeth spanning (a): 0.0° - (b): 11.25° - (c): 22.5°

4.2 Design optimization

In this case, we consider the slots rectangular. A design optimization has been carried out to maximize the value of the available force in the airgap of each tooth. The size of the shaft and the external diameter of the stator are fixed. The aim is to evaluate the best ratio between the three heights: stator yoke height, h_{yoke}, tooth height, h_{tooth}, and rotor lamination height, h_{rot_iron}. h_{rot_iron} can be expressed as a function of h_{yoke} and h_{tooth}. Thus, only two variables are tested. In addition, we consider that the surface of the winding window, $S_{winding}$, is fixed by the product $h_{winding}$. $w_{winding}$, with $h_{winding}$ = h_{tooth} - 4mm, the height of the winding and $w_{winding}$ the width of the winding.

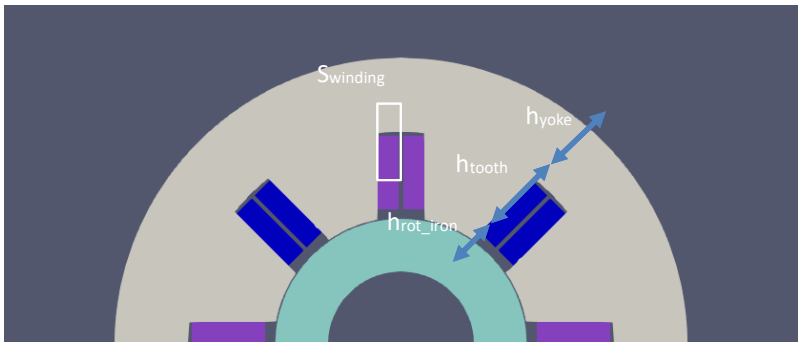

Figure 7 Optimized dimensions of the magnetic bearing

To achieve the optimization, we used the 3DVar technic available in the module ADAO of the Salome platform [5]. This classical and robust algorithm in static data assimilation, performs a state estimation by variational minimization of the objective function J [8]:

$$\mathrm{J}(\mathbf{x}) = \left(\mathbf{x}-\mathbf{x}^{\mathrm{b}}\right)^{\mathrm{T}}\mathbf{B}^{-1}\left(\mathbf{x}-\mathbf{x}^{\mathrm{b}}\right) + \left(\mathbf{y}-\mathbf{y}^{\mathrm{obs}}\right)^{\mathrm{T}}\mathbf{R}^{-1}\left(\mathbf{y}-\mathbf{y}^{\mathrm{obs}}\right) \quad (2)$$

The objective function is the sum of two terms, one measuring the distance to the background x^b, the other measuring the distance to the additional observation vector y^{obs}. These two terms are weighted by the inverse covariance matrices of the corresponding error B and R [8].

For the chosen external diameter of the stator, the optimized dimensions are given in **Table 1**:

Table 1 Obtained dimensions for the magnetic bearing parts in two cases

	Dimensions	*Case 1*	*Case 2*
D_{ext_stator}	External stator diameter	240.0mm	300.0mm
D_{int_stator}	Internal stator diameter	122.0mm	141.8mm
D_{ext_rotor}	External rotor diameter	121.0mm	140.8mm
D_{int_rotor}	Internal rotor diameter	55.0mm	55.0mm
h_{teeth}	Slot height	32.3mm	39.5mm
w_{slot} encoche	Slots width	24.5mm	19.4mm

If we compute the ratio of the stator and rotor iron part of the magnetic bearing, according to the external stator diameter excluding casing, we obtain:

Table 2 ratio of stator and rotor part over the external diameter

	Case 1	*Case2*
stator iron height ratio	49,2%	52,7%
rotor iron height ratio	27,5%	28,6%
rotor shaft diameter+airgap ratio	23,3%	18,7%
Height tooth ratio	13,5%	13,2%

The tooth height ratio remains the same in the two cases. As the external diameter value increases, the ratio on the stator side becomes greater than in the rotor part of the bearing. The forces obtained are given in Figure 8. As the

external stator diameter increases, the value of the forces increases. This can be linked to the fact that both the surface in the airgap where forces are developed increases and the saturation in the magnetic material decreases.

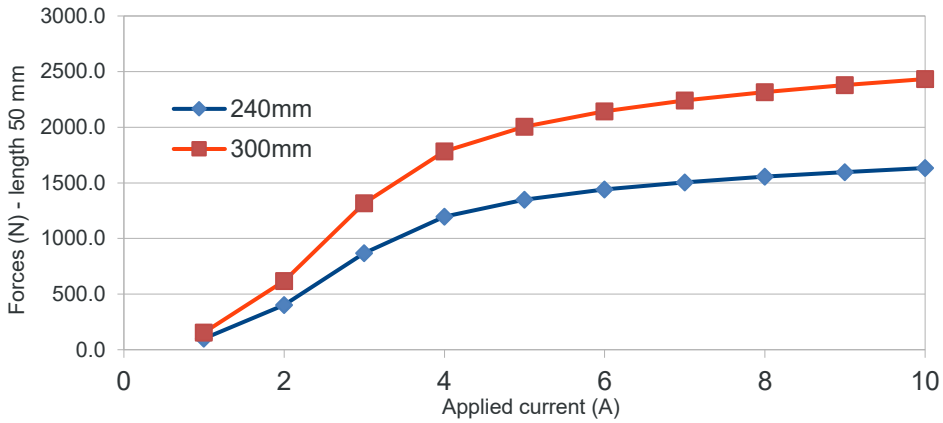

Figure 8 Calculated forces on one tooth for two external stator diameters with optimized dimensions

4.3 Misalignment force

In order to control rotor misalignment within the SAHJB, we have to apply a torque of 86 N.m. The value was predicted by the TEHD model and the detail are out of the scope of the present paper. Considering the dimensions of the rotor, the static forces to be applied by the AMBs is 235.6N.

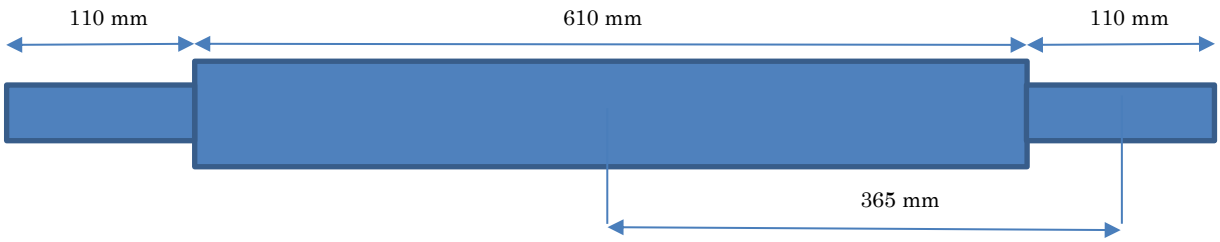

Figure 9 Rotor shaft dimensions used

The value of this force is quite small compares to the static force needed to load the SAHJB and don't appear to be dimensioning. The variation of the airgap is of bigger concerns.

4.4 Evaluation of the effect of misalignment of the rotor shaft

In the case of self-alignment of the SAHJB, we consider that the rotor tilts of 0.04°. Thus, we can estimate the variation of the airgap on each magnetic bearing considering the dimensions of the bench.

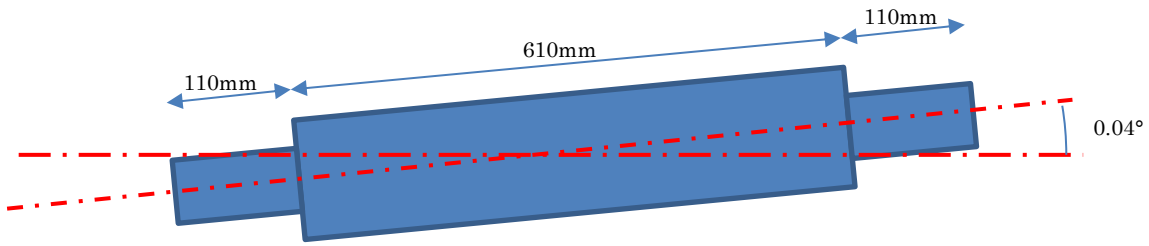

Figure 10 Dimensions used to evaluate the effect of a misalignment of the rotor after SAHJB tilted

The value of the airgap reduction in the middle of the bearing is around 0.256mm and we will use this value to evaluate the effect of the airgap variation on the available forces on each tooth. A 3D study must be done in order to fully estimated the effect but as a first approach, we used a 2D approach considering a mean reduction of 0.256 mm along the full length of the bearing. We consider that the variation of the airgap is anti-symmetrical on the two bearings.

Results obtained are depicted in Figure 11. We can observe, for a given applied current value, the effect of the variation of the airgap size on the y direction with both an increase of the forces where the airgap is reduced and a decrease of the forces where the airgap value is increased. Hence, we will have to consider the variation of the forces into the control part of the bearing.

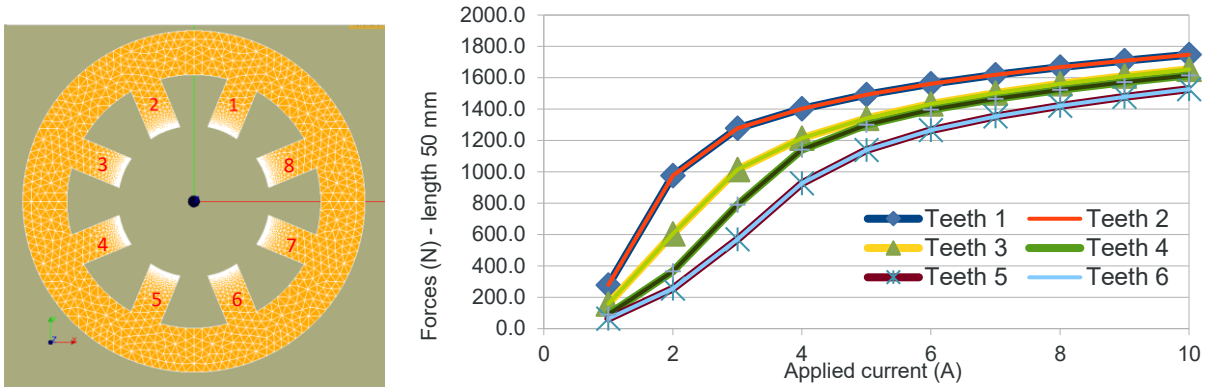

Figure 11 Effect of an airgap reduction of 200 µm on the y direction

5 Conclusions and perspectives

A first modelling has been carried out to evaluate the size of the magnetic bearing needed to be added on both sides of the SAHJB. An optimization technic associated with a parametric CAD drawing and meshing are available to test other dimensions and material in order to achieve the target forces required both by the stability of the rotor and the test of the SAHJB in align or misalign configuration. Further investigations are ongoing to obtain the final design of the AMBs.

A first prototype of the simple electromagnet actuator has been made to validate the modeling done. At this stage, static testing was performed to validate the geometrical design. Testing in real operating conditions are planned where power amplifiers, controllers and sensors design will be considered.

6 References

[1] Hassini, M., Zhang, S., Chatterton, S., and Pennacchi, P. (November 28, 2022). "Theoretical and Experimental Comparisons for Rotordynamic Coefficients of a Multiscratched Tilting Pad Journal Bearing." ASME. J. Eng. Gas Turbines Power. February 2023; 145(2): 021008. https://doi.org/10.1115/1.4055482

[2] Chatterton, S, Pennacchi, P, Vania, A, Hassini, MA, & Kuczkowiak, A. "Effect of Scratches on a Tilting-Pad Journal Bearing." *Proceedings of the ASME Turbo Expo 2020: Turbomachinery Technical Conference and Exposition*. *Volume 10B: Structures and Dynamics*. Virtual, Online. September 21–25, 2020. V10BT29A006. ASME. https://doi.org/10.1115/GT2020-14700

[3] Jolly P, Hassini MA, Arghir M, Bonneau O. Identification of stiffness and damping coefficients of hydrostatic bearing with angled injection. Proceedings of the Institution of Mechanical Engineers, Part J: Journal of Engineering Tribology. 2013;227(8):905-911. doi:10.1177/1350650113482613

[4] Voigt, A. J., Mandrup-Poulsen, C., Nielsen, K. K., and Santos, I. F. (January 4, 2017). "Design and Calibration of a Full Scale Active Magnetic Bearing Based Test Facility for Investigating Rotordynamic Properties of Turbomachinery Seals in Multiphase Flow." ASME. *J. Eng. Gas Turbines Power*. May 2017; 139(5): 052505. https://doi.org/10.1115/1.4035176

[5] Salome platform - https://www.salome-platform.org/

[6] Gerhard Schweitzer and Eric H. *Maslen Magnetic Bearings: Theory, Design, and application to rotating* machinery Springer (2009).

[7] Der Hagopian, J. and Mahfoud, J., "Electromagnetic Actuator Design for the Control of Light Structures", Smart Structures and Systems, Vol. 6, No. 1 (2010), 29-38.

[8] Talagrand O., Assimilation of Observations, an Introduction, Journal of the Meteorological Society of Japan, 75(1B), pp.191-209, 1997